Loss of leucine-rich repeat kinase 2 causes impairment of protein degradation pathways, accumulation of α-synuclein, and apoptotic cell death in aged mice

Youren Tong[a], Hiroo Yamaguchi[a], Emilie Giaime[a], Scott Boyle[b], Raphael Kopan[b], Raymond J. Kelleher III[c], and Jie Shen[a,1]

[a]Center for Neurologic Diseases, Department of Neurology, Brigham and Women's Hospital, Program in Neuroscience, Harvard Medical School, Boston, MA 02115; [b]Department of Developmental Biology, Washington University School of Medicine, St. Louis, MO 63110; and [c]Center for Human Genetic Research, Department of Neurology, Massachusetts General Hospital, Program in Neuroscience, Harvard Medical School, Boston, MA 02115

Edited* by Gregory A. Petsko, Brandeis University, Waltham, MA, and approved April 19, 2010 (received for review April 7, 2010)

Mutations in leucine-rich repeat kinase 2 (LRRK2) are the most common genetic cause of Parkinson's disease. LRRK2 is a large protein containing a small GTPase domain and a kinase domain, but its physiological role is unknown. To identify the normal function of LRRK2 in vivo, we generated two independent lines of germ-line deletion mice. The dopaminergic system of *LRRK2*$^{-/-}$ mice appears normal, and numbers of dopaminergic neurons and levels of striatal dopamine are unchanged. However, *LRRK2*$^{-/-}$ kidneys, which suffer the greatest loss of LRRK compared with other organs, develop striking accumulation and aggregation of α-synuclein and ubiquitinated proteins at 20 months of age. The autophagy–lysosomal pathway is also impaired in the absence of LRRK2, as indicated by accumulation of lipofuscin granules as well as altered levels of LC3-II and p62. Furthermore, loss of LRRK2 dramatically increases apoptotic cell death, inflammatory responses, and oxidative damage. Collectively, our findings show that LRRK2 plays an essential and unexpected role in the regulation of protein homeostasis during aging, and suggest that LRRK2 mutations may cause Parkinson's disease and cell death via impairment of protein degradation pathways, leading to α-synuclein accumulation and aggregation over time.

Parkinson's disease | knockout | autophagy | ubiquitin-proteasome system | aging

Parkinson's disease (PD) is the most common movement disorder. The neuropathological hallmarks of PD are progressive degeneration of dopaminergic (DA) neurons and the presence of intraneuronal cytoplasmic inclusions known as Lewy bodies, of which α-synuclein is a major constituent (1). Dominantly inherited mutations in leucine-rich repeat kinase 2 (LRRK2) are the most common cause of familial PD (2, 3), highlighting the importance of LRRK2 in PD pathogenesis; however, the normal physiological role of LRRK2 is unknown. LRRK2 is a large protein containing a Ras-like small GTPase domain and a MAPKKK-like kinase domain, and has a functional homolog LRRK1, which shares similar domain structures (4). Crystal structural and biochemical studies showed that the GTPase domain forms a dimer; the pathogenic mutations destabilize the dimer and reduce GTPase activity (5–7). A recent in vitro study suggested that LRRK2 and LRRK1 can interact with each other and form a heterodimer (8). Although no physiological substrate of the LRRK2 kinase activity has been reported, studies in cultured cells have suggested that some pathogenic mutations in LRRK2 cause increases in LRRK2 kinase activity (9, 10).

Protein aggregation is thought to play a major role in neurodegeneration and PD pathogenesis (11). The strongest evidence came from studies of α-synuclein. Gene multiplication and missense mutations in α-synuclein have been identified in early-onset familial PD with dominant inheritance (12). α-Synuclein is a major constituent of Lewy bodies (1). Overexpression of either WT or mutant α-synuclein in transgenic mice causes age-related neurodegeneration (13–15). Although patients carrying recessively inherited mutations in *Parkin* often do not have Lewy bodies (no reports of postmortem studies on *DJ-1* and *PINK1* yet), PD patients bearing mutations in *α-synuclein* or *LRRK2* typically have Lewy bodies in nigral neurons (16).

To elucidate the normal physiological role of LRRK2 in vivo, we generated two independent lines of *LRRK2* germ-line deletion mice. Although *LRRK2*$^{-/-}$ mice do not develop apparent neurodegeneration and neuropathological changes in the brain, loss of LRRK2 causes striking age-dependent accumulation and aggregation of α-synuclein (60-fold) and ubiquitinated proteins in the kidney, in which LRRK2 is normally expressed at high levels (~6-fold compared to the brain). The autophagy–lysosomal pathway is also impaired in the absence of LRRK2, and there are dramatic increases in apoptotic cell death, inflammatory responses, and oxidative damage. These results demonstrate an essential cellular function of LRRK2 during aging in the maintenance of protein homeostasis and, specifically, α-synuclein through the regulation of protein degradation pathways.

Results

Generation and Molecular Characterization of *LRRK2*$^{-/-}$ Mice. We generated two independent lines of *LRRK2* germ-line deletion mice, targeting the promoter and exon 1 in knockout 1 (KO1) and exons 29 and 30, which encode the first half of the Ras-like small GTPase domain, in *LRRK2* KO2. The targeting strategies for the generation of KO1 and KO2 are shown in Fig. 1*A* and Fig. S1*A*, respectively. The linearized targeting vectors were transfected by electroporation into MKV6.5 ES cells, which were derived from F1 hybrid of B6 and 129 mice. ES cell clones were screened by Southern blotting using the 5′ external probe to identify those carrying the proper homologous recombination event, which were further confirmed by Southern blotting using the 3′ external and the *neo* probes. Southern blotting analysis of tail genomic DNAs of heterozygous F1 and homozygous F2 (Fig. 1*B* and Fig. S1*B*) mice confirmed the germ-line transmission of the targeted alleles.

We then deleted the floxed *PGK-neo* cassette by crossing the homozygous F2 mice with *CaMKII-cre* transgenic mice, in which Cre is expressed in male gametes, resulting in excision of the floxed *PGK-neo* cassette. Southern blotting confirmed the deletion of the floxed *PGK-neo* selection cassette in homozygous KO1 (Fig. 1*C*) and KO2 (Fig. S1*C*) mice. Northern analyses of

Author contributions: Y.T. and J.S. designed research; Y.T., H.Y., E.G., and S.B. performed research; Y.T., H.Y., E.G., S.B., R.J.K., and J.S. analyzed data; and Y.T. and J.S. wrote the paper.

The authors declare no conflict of interest.

*This Direct Submission article had a prearranged editor.

[1]To whom correspondence should be addressed. E-mail: jshen@rics.bwh.harvard.edu.

This article contains supporting information online at www.pnas.org/lookup/suppl/doi:10.1073/pnas.1004676107/-/DCSupplemental.

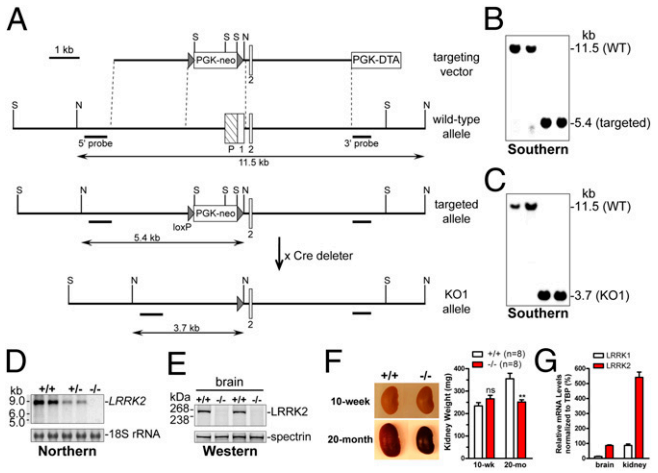

Fig. 1. Age-dependent renal atrophy in *LRRK2*$^{-/-}$ mice. (*A*) Targeting strategy for generation of *LRRK2* KO1 mice. The locations of the 5′ and 3′ external probes used for Southern blotting are indicated. Restriction site: N, NheI; S, SphI. (*B* and *C*) Southern blotting of tail genomic DNAs using 5′ probe shows germ-line transmission of targeted allele (*B*) and KO1 allele (*C*). Tail genomic DNAs were digested with NheI. The 11.5-kb band represents the WT allele, whereas the 5.4-kb and 3.7-kb bands represent the targeted allele and KO1 allele, respectively. (*D*) Northern blotting of total RNAs from brains of KO1 mice shows absence and reduction of *LRRK2* mRNAs in $^{-/-}$ and $^{+/-}$ mice, respectively. A 406-bp cDNA fragment spanning exons 1–5 of *LRRK2* was used as a probe. 18S rRNAs were used as loading control. (*E*) Western blotting indicates absence of LRRK2 in the brain of $^{-/-}$ mice. Reprobing of the same membranes with an antibody specific for spectrin was used as loading control. (*F*) Compared with WT controls, kidneys (fresh, nonperfused) from 20-month-old *LRRK2*$^{-/-}$ mice are significantly smaller and darker and weigh ∼30% less, whereas kidneys (perfused) from 10-week-old *LRRK2*$^{-/-}$ mice are similar in size and weight to WT controls. $n = 8$ Kidneys per genotypic group. (*G*) Quantitative RT-PCR showing relative expression levels of *LRRK1* and *LRRK2* mRNAs, after normalized to an internal control TATA-binding protein (*TBP*) mRNA, in the brain and kidney of WT mice ($n = 3$). All data are expressed as mean ± SEM. ns, Not significant. $^{**}P < 0.01$.

total RNAs from brains of mice using a cDNA probe specific for exons 1–5 (KO1) or specific for exons 29–30 (KO2) indicate the absence of *LRRK2* mRNAs (Fig. 1*D* and Fig. S1*D*). Western blotting confirmed the absence of LRRK2 protein in the brain of KO1 and KO2 mice (Fig. 1*E* and Fig. S1*E*). Thus, we conclude that the KO1 and KO2 alleles are null alleles ($^{-/-}$). Because similar results were obtained from both KO1 and KO2 mice, the data shown below are all from the analysis of KO1 mice.

Absence of DA Neurodegeneration and Neuropathological Changes in *LRRK2*$^{-/-}$ Mice. To determine whether the deletion of LRRK2 causes degeneration of dopaminergic neurons, we performed immunohistochemical analysis using an antibody specific for tyrosine hydroxylase. The morphology of dopaminergic neurons (Fig. S1*F*) and their projections (Fig. S1*G*) appeared grossly normal in *LRRK2*$^{-/-}$ mice. Quantitative analysis of tyrosine hydroxylase–immunoreactive neurons in the substantia nigra pars compacta using stereological methods revealed normal numbers of dopaminergic neurons in *LRRK2*$^{-/-}$ mice at 2 years of age (Fig. S1*H*). We also measured the levels of striatal dopamine and its major metabolites using HPLC. The steady-state striatal dopamine level was not significantly changed in *LRRK2*$^{-/-}$ mice at the ages of 3 months, 1 year, and 2 years (Fig. S1*I*), compared with their WT littermate controls. There was also no significant alteration in the striatal levels of major metabolites of dopamine, dihydroxylphenylacetic acid, and homovanillic acid in *LRRK2*$^{-/-}$ mice at 2 years of age (Fig. S1*I*), suggesting normal dopamine turnover.

We did not observe abnormal accumulation and aggregation of α-synuclein (Fig. S2*A*) and ubiquitin (Fig. S2*B*) in *LRRK2*$^{-/-}$ brains at 2 years of age. There was also no apparent increase in astrocytosis or microgliosis, normally associated with neurodegeneration, in any brain subregions of *LRRK2*$^{-/-}$ mice at 2 years of age, as shown by normal immunoreactivity for glial fibrillary acidic protein (GFAP) (Fig. S3*A*) and ionized calcium binding adaptor molecule 1 (Iba1) (Fig. S3*B*). Neuronal structures shown by MAP2 and synaptophysin immunoreactivity appeared normal in *LRRK2*$^{-/-}$ mice.

Striking Age-Dependent Renal Atrophy in *LRRK2*$^{-/-}$ Mice. As *LRRK2*$^{-/-}$ mice age, they develop striking age-dependent abnormalities in the kidney. At 10 weeks of age, *LRRK2*$^{-/-}$ kidneys were normal in morphology and weight, but by 20 months of age, *LRRK2*$^{-/-}$ kidneys appeared significantly smaller in size and much darker in color and weighed 31% less (Fig. 1*F*), whereas the body weights of *LRRK2*$^{-/-}$ mice were not significantly different from those of WT controls. In addition, the surface of the aged *LRRK2*$^{-/-}$ kidney appeared rough and granular. These changes in kidneys were observed in both KO1 and KO2 lines with 100% penetrance, but not in our LRRK2 R1441C knockin mice. Despite these dramatic morphological changes in the kidney, we did not observe any gross changes in other organs of *LRRK2*$^{-/-}$ mice up to 2 years of age. Thus, the loss of LRRK2 causes striking age-dependent alteration specifically in the kidney, which may be explained by the fact that LRRK2 is normally expressed at much higher levels in the kidney (∼6.2-fold) relative to the brain (Fig. 1*G*) and other organs (17).

Accumulation and Aggregation of α-Synuclein and Ubiquitinated Proteins. To uncover the mechanism underlying age-related abnormalities developed in older *LRRK2*$^{-/-}$ mice, we performed a number of analyses to look for molecular and cellular alterations. Western blotting showed an ≈60-fold increase in the level of α-synuclein in Triton X-100–soluble fractions of kidneys from 20-month-old *LRRK2*$^{-/-}$ mice (Fig. 2 *A* and *B*) , indicating dramatic accumulation of α-synuclein in the absence of LRRK2, whereas α-synuclein was normally present at very low levels in the kidney (∼1/200 compared with the brain). Furthermore, levels of higher-molecular-weight (HMW) species immunoreactive to α-synuclein–specific antibodies were also increased in Triton-insoluble fractions from these *LRRK2*$^{-/-}$ kidneys (Fig. 2 *A* and *B*), indicating aggregation of α-synuclein in the absence of LRRK2.

Consistent with findings from Western blotting, immunohistochemical analysis showed widely distributed cytosolic α-synuclein–immunoreactive granular aggregates or inclusions in boxy cells of renal tubules in the cortical area of *LRRK2*$^{-/-}$ kidneys at 20 months of age (Fig. 2 *C* and *D*), which were not present in kidneys of WT controls or *LRRK2*$^{-/-}$ mice at 10 weeks of age. These data together suggest an age-dependent accumulation and aggregation of α-synuclein in the absence of LRRK2.

α-Synuclein is phosphorylated at the residue Ser-129 in synucleinopathy lesions, and phosphorylation of α-synuclein at Ser-129 has been reported to promote aggregation of α-synuclein in vitro (18). Immunohistochemical analysis using an antibody specific for α-synuclein phosphorylated at Ser-129 also revealed granular aggregates or inclusions in kidneys of *LRRK2*$^{-/-}$ mice at 20 months of age (Fig. 2 *C* and *D*) but not in kidneys of WT controls or young *LRRK2*$^{-/-}$ mice, indicating increased levels of phospho-Ser-129 α-synuclein, which likely contribute to α-synuclein aggregation.

We further examined whether the ubiquitin–proteasome system (UPS)–mediated protein degradation is affected in aged *LRRK2*$^{-/-}$ kidneys. Western blotting showed dramatically increased levels of HMW protein species immunoreactive for ubiquitin-specific antibody in Triton X-100–insoluble fractions of kidneys from aged *LRRK2*$^{-/-}$ mice (Fig. 2 *A* and *B*), suggesting accumulation and aggregation of ubiquitinated proteins in the absence of LRRK2. Consistent with this finding, immunohisto-

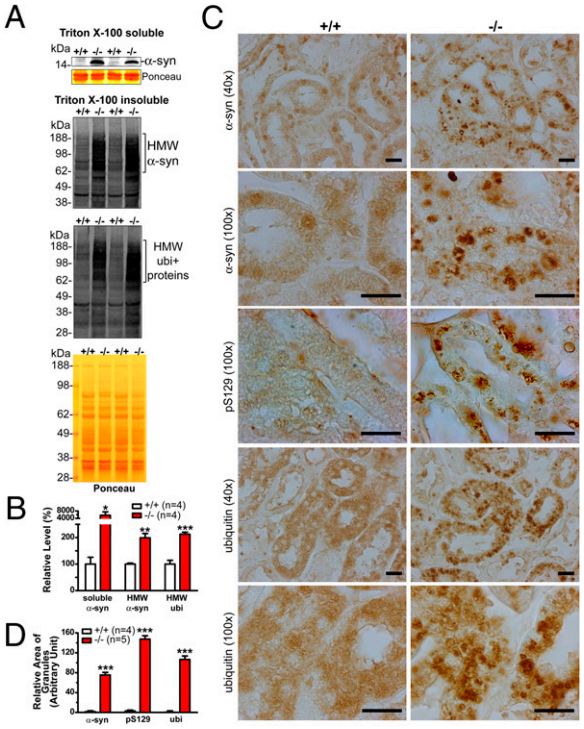

Fig. 2. Accumulation and aggregation of α-synuclein and ubiquitinated proteins in absence of LRRK2. (*A*) Representative Western blots showing dramatically increased levels of α-synuclein monomers (soluble α-syn) in Triton X-100–soluble fractions and HMW α-synuclein species (HMW α-syn) and ubiquitin-positive proteins (HMW ubi+) in Triton X-100 insoluble fractions in kidneys of 20-month-old *LRRK2*$^{-/-}$ mice. Ponceau S staining is used as loading control, as levels of β-actin are altered in *LRRK2*$^{-/-}$ kidneys. (*B*) Quantification of Triton-soluble α-synuclein monomers and insoluble HMW α-synuclein and ubiquitin-positive proteins (bracketed region) from Western blots as shown in *A*. (*C*) Immunohistochemical analysis shows widely distributed cytosolic granules or inclusions immunoreactive to α-synuclein-, phospho–α-synuclein–specific (pS129), or ubiquitin-specific antibody in boxy cells of renal tubules in kidneys of 20-month-old *LRRK2*$^{-/-}$ mice. (All scale bars, 20 μm.) (*D*) Relative areas of granules immunoreactive to α-synuclein–specific (α-syn), phospho–α-synuclein–specific (pS129), or ubiquitin (ubi)–specific antibody as shown in *C* were estimated using the ImageJ program (National Institutes of Health). Data in all panels are expressed as mean ± SEM. **P* < 0.05; ***P* < 0.01; ****P* < 0.001.

chemical analysis revealed widely distributed cytosolic granules or inclusions immunoreactive to ubiquitin-specific antibody in kidneys of aged *LRRK2*$^{-/-}$ mice (Fig. 2 *C* and *D*), which were barely detectable in WT controls and in kidneys of young *LRRK2*$^{-/-}$ mice. These results suggest that UPS-mediated protein degradation is impaired in the absence of LRRK2.

Impaired Autophagy–Lysosomal Pathway in Aged *LRRK2*$^{-/-}$ Mice. We then performed histological analysis using Periodic Acid-Schiff and Sudan Black B, which stain macromolecules containing carbohydrates and lipids, respectively. Periodic Acid-Schiff staining showed significantly darker pink staining in renal tubules and glomeruli in the cortex of *LRRK2*$^{-/-}$ kidneys at 20 months of age (Fig. 3*A*). Sudan Black B staining further revealed dark brown granules, which show bright autofluorescence, suggesting abnormal accumulation of lipofuscin granules in kidneys of aged *LRRK2*$^{-/-}$ mice (Fig. 3*A*). Lipofuscin granules are composed of undigested materials from lysosomes containing oxidized lipids, carbohydrates and proteins, and are undegraded aggregates as a result of excessive oxidation and crosslinking (19). Consistent with this finding, levels of protein carbonyls, a general marker of oxidative damage, were also increased in kidneys of 20-month-old *LRRK2*$^{-/-}$ mice (Fig. 3*B*). Abnormal accumulation of lipofuscin granules suggests impairment of the autophagy–lysosomal system and has been implicated in neurodegenerative disorders such as PD.

To assess further autophagy function in the absence of LRRK2, we evaluated markers of autophagosomes, such as microtubule-associated protein 1 light chain 3 (LC3), a homolog of Atg8, which is essential for autophagy function in yeast (20, 21). There are two forms of LC3, I and II. LC3-II is the lipidated form of LC3-I and is bound to autophagosomal membranes. The amount of LC3-II correlates with the extent of autophagosome formation, and the conversion of LC3-I to LC3-II is a reliable indicator of autophagic activity (22). Western analysis showed that levels of LC3-II are dramatically decreased in *LRRK2*$^{-/-}$ kidneys at 20 months of age (Fig. 3*C*), indicating impaired autophagosome formation in the absence of LRRK2. The higher level of LC3-I in *LRRK2*$^{-/-}$ mice (Fig. 3*C*) suggests altered LC3-I to LC3-II conversion, further supporting reduced autophagic activity in the absence of LRRK2.

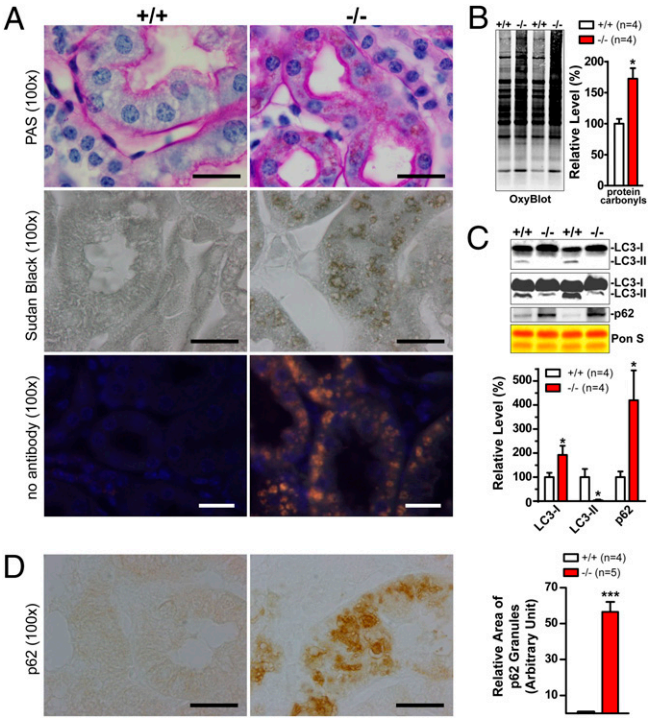

Fig. 3. Impairment of the autophagy–lysosomal pathway and increases in oxidative damage. (*A*) Periodic Acid-Schiff staining of cross sections of kidneys shows thicker and darker pink staining in renal tubules and the presence of widely distributed brown granules in boxy cells of renal tubules of 20-month-old *LRRK2*$^{-/-}$ mice compared with WT controls ($^{+/+}$). Nuclei were counterstained with hematoxylin (blue). Sudan Black B staining reveals, in renal tubules of *LRRK2*$^{-/-}$ mice, widely distributed dark brown granules that show bright autofluorescence (orange for merged fluorescence) in the absence of any primary and secondary antibodies. (*B*) Elevated levels of protein carbonyls (OxyBlot) in Triton X-100–insoluble fractions of kidneys from 20-month-old *LRRK2*$^{-/-}$ mice. Equal loading of total proteins was confirmed by Ponceau S–staining of the membranes. (*C*) Western blotting shows dramatically decreased levels of autophagosome marker LC3-II (some LC3-II signals are detected when more proteins were loaded and longer exposure was used) and increased levels of an autophagy substrate p62 in Triton X-100–insoluble fractions of kidneys from *LRRK2*$^{-/-}$ mice. (*D*) Immunohistochemical analysis revealed the presence of granular aggregates or inclusions immunoreactive to p62-specific antibody in the deeper layer of the renal cortex of *LRRK2*$^{-/-}$ mice. Relative areas of granules immunoreactive to p62 antibody were estimated using the ImageJ program (National Institutes of Health). (All scale bars, 20 μm.) Data in all panels are expressed as mean ± SEM. **P* < 0.05; ****P* < 0.001.

NEUROSCIENCE

Inhibition of autophagy by inactivation of Atg7, a protein essential for autophagy function (23), leads to drastically elevated levels of p62 in *Atg7* conditional KO mice (24). We found that levels of p62 were significantly higher in aged *LRRK2*$^{-/-}$ mice (Fig. 3*C*). Immunohistochemical analysis showed dramatically increased numbers of p62-immunoreactive granules in the cortex of kidneys from 20-month-old *LRRK2*$^{-/-}$ mice (Fig. 3*D*). Interestingly, the strongest p62-immunoreactive granular signals in kidneys of *LRRK2*$^{-/-}$ mice appeared to be localized in the deeper layer of the renal cortex and the boundary region between the cortex and medulla, where *LRRK2* mRNA is most highly expressed in WT kidneys and *LRRK1* mRNAs were almost undetectable (25). These results further demonstrate impairment of autophagy function in the absence of LRRK2.

Increased Apoptosis and Inflammation in Aged *LRRK2*$^{-/-}$ Mice. To examine the consequence of impaired UPS and autophagy as well as accumulation and aggregation of α-synuclein, we looked for possible degeneration in kidneys of *LRRK2*$^{-/-}$ mice at 20 months of age, which may explain the 30% weight reduction. Immunohistochemical analysis revealed dramatic increases in the number of apoptotic cells labeled by TUNEL assay and active caspase-3 immunoreactivity in medulla, renal tubules, and glomeruli of kidneys from 20-month-old *LRRK2*$^{-/-}$ mice compared with WT controls (Fig. 4 *A* and *B*) . Few cells were immunoreactive for active caspase-3 in *LRRK2*$^{-/-}$ mice at 10 weeks of age. Western blotting showed elevated levels of the active forms of caspase-3 and caspase-6 (Fig. 4*C*), two effector caspases in apoptosis, providing further support for increased apoptotic cell death in the absence of LRRK2.

Because degeneration is often accompanied by inflammatory responses, we further looked at markers for inflammatory responses in *LRRK2*$^{-/-}$ kidneys. Immunohistochemical analysis revealed striking up-regulation of cathepsin S and complement C1q (Fig. 4 *D* and *E*), widely used markers for inflammatory responses (26, 27), in kidneys of *LRRK2*$^{-/-}$ mice at 20 months of age, whereas levels of these markers in kidneys of *LRRK2*$^{-/-}$ mice at 10 weeks of age were normal. Western analysis also confirmed the increases in the levels of cathepsin S and C1q in kidneys of 20-month-old *LRRK2*$^{-/-}$ mice (Fig. 4*F*). Histological and immunohistochemical analyses also showed large clusters of invading B cells and accumulation of endogenous mouse Ig around these B cell clusters in kidneys of 20-month-old *LRRK2*$^{-/-}$ mice.

Discussion

Mutations in LRRK2 are the most common genetic cause of PD, but its function in the cell has remained unknown. In the current study, our genetic analysis revealed an unexpected cellular role of LRRK2 in protein homeostasis. Specifically, loss of LRRK2 causes dramatic accumulation and aggregation of α-synuclein and ubiquitinated proteins in an age-dependent manner (Fig. 2) as well as impairment of the autophagy–lysosomal pathway (Fig. 3). These age-dependent abnormalities are accompanied by increases in apoptotic cell death, inflammatory responses, and oxidative damage (Figs. 3 and 4). Interestingly, these cellular changes bear striking resemblance to processes that are thought to be involved in PD pathogenesis, such as α-synuclein aggregation (1), apoptosis and autophagic degeneration (28), impairment of the ubiquitin–proteasome pathway, and accumulation of oxidized proteins (29).

How does loss of LRRK2 lead to these PD-like changes? Defects in the protein degradation pathways are the likely culprit. The ubiquitin–proteasome pathway may be affected, as suggested by dramatic increases in ubiquitinated proteins in the kidney of aged *LRRK2*$^{-/-}$ mice (Fig. 2). Interestingly, α-synuclein is affected by 60-fold accumulation of total α-synuclein and formation of α-synuclein aggregates in the kidney of aged *LRRK2*$^{-/-}$ mice (Fig. 2). Furthermore, the autophagy–lysosomal pathway is impaired, as indicated by reduced levels of LC3-II (Fig. 3), which is considered the most reliable indicator of autophagic activity (22). The impairment of autophagy function is further supported by increased levels of p62 (Fig. 3), consistent with previous findings showing that suppression of autophagy function by Atg7 inactivation caused accumulation of p62 (24). Given the fact that inhibition of autophagy has been reported to induce apoptotic cell death in various cell types including neurons and T cells (30–32), impairment of autophagy caused by loss of LRRK2 likely underlies or contributes to the increased apoptotic cell death in *LRRK2*$^{-/-}$ mice.

There is accumulating evidence indicating that there is a crosstalk between autophagy and the UPS. For example, suppression of autophagy function by Atg5 or Atg7 inactivation causes accumulation of ubiquitin-positive inclusions and UPS substrates (24, 30, 31, 33). Deletion of p62, which binds LC3 and ubiquitin, prevents the formation of ubiquitin-positive protein aggregates caused by autophagy inactivation (24, 33). Overexpression of p62 in cultured cells resulted in increased levels of mutant α-synuclein (A53T) (33). Thus, accumulation and aggregation of α-synuclein in our *LRRK2*-deficient mice may be a consequence of impaired autophagy and UPS functions. Future research will be needed to resolve whether LRRK2 controls UPS function directly or via its regulation of the autophagy pathway.

Despite these striking age-related changes in *LRRK2*$^{-/-}$ mice that are very relevant to PD pathogenesis, one might question why similar phenotypes are missing in the brain (Figs. S1–S3). The simplest explanation is that LRRK1, a functional homolog of LRRK2, may compensate functionally for the loss of LRRK2 in brains of *LRRK2*$^{-/-}$ mice. *LRRK1* mRNAs are broadly expressed in the developing and adult brain, and the expression level of *LRRK1* in the developing brain is much higher than that of *LRRK2* (25). The specific abnormalities in *LRRK2*$^{-/-}$ kidneys are likely due to the much higher level of *LRRK2* mRNAs normally expressed in the kidney (Fig. 1*G*) compared with other organs (e.g., ~6-fold higher than in the brain) (17). There is no compensatory up-regulation of LRRK1 in the absence of LRRK2. Interestingly, in the deeper cortical region of the kidney, where *LRRK2* mRNAs are most highly expressed and *LRRK1* mRNAs are least abundant (25), we observed the strongest granular accumulation of p62. These results suggest that the LRRK family (LRRK1 and LRRK2) plays an essential role in the regulation of protein homeostasis, and that the *LRRK2*$^{-/-}$ kidney suffers the biggest loss of LRRK compared with other organs, and thereby develops the most striking age-dependent abnormalities as a consequence of impaired protein degradation pathways. Therefore, it will be necessary to generate *LRRK1*/*LRRK2* double KO to determine whether complete loss of LRRK in neurons, especially in DA neurons where oxidative stress is elevated, results in age-related α-synuclein aggregation, autophagy impairment, and neuronal degeneration.

Another important issue that is worth discussing is why loss of LRRK2 function causes alterations that are strikingly similar to PD, whereas only dominantly inherited missense mutations have been found in familial and sporadic PD cases (12). The lack of deletion and nonsense mutations and the dominant inheritance argue against a simple loss-of-function pathogenic mechanism, and suggest that mutant LRRK2 may act in a dominant negative manner to inhibit function of WT LRRK2. Several lines of recent experimental evidence are in support of this notion. For example, crystal structural analysis revealed that the ROC (for Ras of complex proteins) GTPase domain forms a dimer, and that mutations at the R1441 (R1441C, R1441G, R1441H) and I1371 (I1371V) residues destabilize the ROC dimer and decrease GTPase activity (5), which is thought to up-regulate the kinase activity (10, 34). Additional biochemical studies provided further support for LRRK2 functioning as a dimer (6, 7). It was also reported that tagged LRRK2 and LRRK1 can interact with

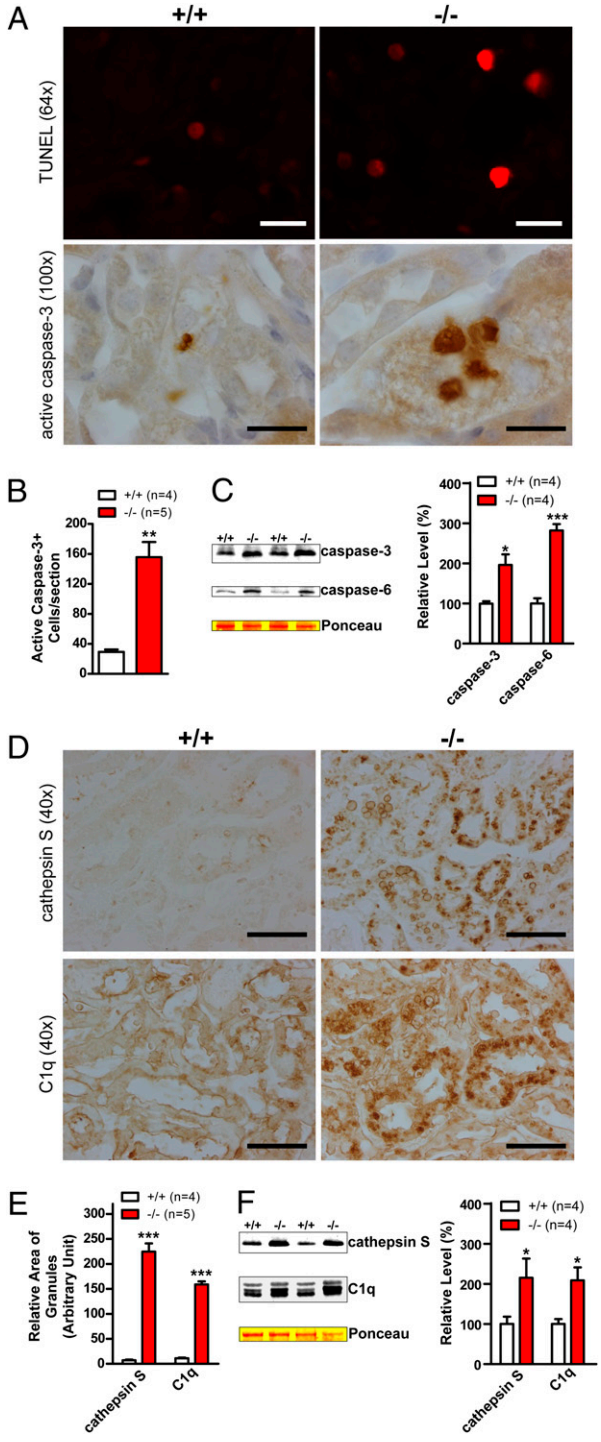

Fig. 4. Increases in apoptotic cell death and inflammatory responses. (*A*) TUNEL and immunohistochemical analysis shows increased numbers of TUNEL-positive cells and densely stained active caspase-3–immunoreactive cells, respectively, in kidneys of 20-month-old *LRRK2*$^{-/-}$ mice. (*B*) Quantification of active caspase-3–immunoreactive cells shows dramatic increases of apoptotic cells in *LRRK2*$^{-/-}$ mice. (*C*) Western analysis shows increased levels of active caspase-3 and caspase-6 in Triton X-100–soluble fractions of *LRRK2*$^{-/-}$ mice. (*D*) Immunohistochemical analysis reveals up-regulation of cathepsin S and complement C1q, two commonly used inflammation markers, in *LRRK2*$^{-/-}$ mice. (*E*) Relative areas of granules immunoreactive to cathepsin S- or C1q-specific antibody were estimated using the ImageJ program (National Institutes of Health). (*F*) Western blotting confirms the elevated level of cathepsin S and C1q in Triton X-100–insoluble fractions of kidneys from 20-month-old *LRRK2*$^{-/-}$ mice. (Scale bars, 20 μm for ×64 and ×100, and 50 μm for ×40.) Data in all panels are expressed as mean ± SEM. $*P < 0.05$; $**P < 0.01$; $***P < 0.001$.

each other and form a heterodimer, and that LRRK1 variants can affect the age of disease onset among LRRK2 mutation carriers (8). Future studies will be needed to determine whether all pathogenic missense mutations in LRRK2 affect dimer formation and reduce GTPase activity, which in turn increases its kinase activity.

Consistent with this partial loss-of-function pathogenic mechanism, expression of various mutant forms of LRRK2 in mice, even at more than 10-fold of overproduction, has so far failed to reproduce PD-like neuropathological changes, such as cell death and α-synuclein aggregation (35–38). Interestingly, a recent report showed that LRRK2 inactivation alleviated rather than exacerbated α-synuclein aggregation and neurodegeneration under overexpression conditions (>16-fold) in α-synuclein transgenic mice (37). However, it was unclear whether autophagy function is affected by α-synuclein overexpression in these transgenic mice. It will be interesting to test whether a huge excess of α-synuclein in the brain of transgenic mice impairs protein degradation pathways, and whether autophagy function is the focal point of the regulation by both α-synuclein overexpression and loss of LRRK2.

In summary, our genetic study demonstrates that LRRK2 controls protein homeostasis in the cell. During the aging process, the *LRRK2*$^{-/-}$ kidney, which suffers the biggest loss of LRRK, develops impairment of protein degradation pathways, leading to huge accumulation of α-synuclein and aggregation. These dramatic molecular and cellular alterations likely underlie increased cell death and inflammatory responses in these mice. Thus, inhibition of LRRK2 function may not represent a suitable therapeutic strategy for the treatment of PD and suppression of α-synuclein aggregation. Future studies will be needed to determine how LRRK2 regulates the autophagy–lysosomal pathway and whether its Ras-like GTPase domain is required for this function. It remains to be tested whether LRRK2 mutations affect autophagy and UPS functions and whether LRRK2 regulates the ubiquitin–proteasome pathway directly or indirectly via autophagy. Crossing *LRRK2*$^{-/-}$ with *α-synuclein*$^{-/-}$ mice will allow us to determine the importance of α-synuclein accumulation and aggregation in the age-dependent cell death and other degenerative processes caused by loss of LRRK2. Targeting protein degradation pathways (e.g., enhancing autophagy) may be a useful venue to pursue for restoring protein homeostasis and treatment of PD.

Materials and Methods

Generation of LRRK2 KO Mice. To generate two independent lines of LRRK2 KO mice, two targeting vectors were constructed. To generate *LRRK2* KO1 mice, a 2.5-kb DNA fragment upstream of the *LRRK2* promoter, and a 3.5-kb DNA fragment encompassing exon 2 as well as part of introns 1 and 2 of *LRRK2,* were amplified by PCR using genomic DNA of C57BL/6J (B6) mice in a BAC clone containing this part of the *LRRK2* gene as template. To generate *LRRK2* KO2 mice, a 2.3-kb DNA fragment encompassing exon 28 and a 3.4-kb DNA fragment encompassing exon 31 were amplified by PCR using tail genomic DNAs of B6 mice as template. These fragments were confirmed by DNA sequencing and used as 5′ and 3′ homologous arms in KO1 and KO2 targeting vectors, respectively. Each linearized targeting vector was transfected by electroporation into MKV6.5 ES cells derived from B6/129 F1 mice. Desired homologous recombination events were confirmed by Southern blotting with the 5′ and 3′ external probes and the neo probe. ES cells from two targeted clones for each KO line were injected into B6 blastocysts. The resulting chimeric mice were mated with B6/129 F1 mice. The homozygous F2 mice obtained from intercrossing of heterozygous F1 mice carrying the targeted allele were mated with *CaMKII-cre* transgenic mice to delete the floxed *PGK-neo* selection cassette to obtain heterozygous mice carrying the KO allele. All animal experimentation followed the protocol approved by Harvard Center for Animal Resources and Comparative Medicine.

Histological and Immunohistochemical Analysis. Mice were anesthetized by i.p. injection of sodium pentobarbital 15 min after injection of heparin. Mice were then transcardially perfused with Ringer's solution containing 0.25 g/L heparin and 5 g/L procaine followed by ice-cold 4% paraformaldehyde in

NEUROSCIENCE

PBS (pH 7.4). The brain and kidneys were postfixed in 4% paraformalhehyde at 4 °C overnight and then processed for paraffin embedding following standard procedures. Sections were cut at 16 μm (brain) or 8 μm (kidney). For histology, sections were stained by Periodic Acid-Schiff stain kit (Dako) or Sudan Black B. For immunohistochemical analysis, some tissue sections were subjected to antigen retrieval by microwaving or autoclaving for 10 or 15 min in 10 mM sodium citrate buffer, pH 6.0. Endogenous peroxidase activity was quenched by incubating in 0.3% H_2O_2. After blocking, sections were incubated with primary antibodies overnight at 4 °C, followed by 1-h incubation with biotinylated secondary antibodies and 1-h incubation with Vectastain Elite ABC reagent, and then developed using chromogenic DAB substrate (Vector Laboratories). For negative controls, primary antibodies, alone or together with secondary antibodies, were omitted from the incubation buffer. Stereological DA neuron counting was performed as previously described (38). Apoptotic cells were detected by a colorimetric TUNEL staining using an in situ cell death detection kit (Roche) following the manufacturer's instructions.

Preparation of Nonionic Detergent-Soluble and Detergent-Insoluble Fractions. Fresh mouse brains or kidneys were homogenized in ice-cold radioimmunoprecipitation assay buffer (50 mM Tris·HCl, pH 7.4, 150 mM NaCl, 0.1% SDS, 1% Triton X-100, 1% sodium deoxycholate, supplemented with protease inhibitor mixture and phosphatase inhibitor mixtures), followed by sonication. Homogenates were centrifuged at 14,000 × *g* for 20 min at 4 °C to separate supernatants (fractions soluble in 1% Triton X-100). The resulting pellets were further lysed with a buffer containing 4% SDS and 20 mM Hepes, pH 7.5, supplemented with protease inhibitor mixture and phosphatase inhibitor mixtures by vortexing and sonication, followed by centrifugation at 19,600 × *g* for 10 min at room temperature to separate the new supernatants (Triton X-100–insoluble fractions).

Western Blotting Analysis and OxyBlot. Equal amounts of total proteins from each preparation were loaded and separated in NuPAGE 3–8% Tris-Acetate gels or 4–12% Bis-Tris gels (Invitrogen) and then transferred to nitrocellulose membranes. Oxyblots for detecting protein carbonyls were prepared following the manufacturer's instructions (Chemicon). After blocking and overnight incubation with primary antibodies, protein bands of interest were visualized by binding of IRDye-labeled secondary antibodies, and band intensity was analyzed using Odyssey imaging system (Li-Cor). Antibodies used are listed in *SI Materials and Methods.*

Statistical Analysis. Statistical analysis was performed using Prism 5 (GraphPad Software) and Excel (Microsoft). Data are presented as means ± SEM. Statistical significance was determined based on *P* values derived from Student's *t* test or two-way ANOVA.

ACKNOWLEDGMENTS. We thank Huailong Zhao and Lan Wang for technical assistance. This work was supported by grants from the National Institute of Neurological Disorders and Stroke and the Michael J. Fox Foundation (to J.S.) and grants from the National Institute of Diabetes and Digestive and Kidney Diseases (to R.K. and S.B.).

1. Spillantini MG, et al. (1997) Alpha-synuclein in Lewy bodies. *Nature* 388:839–840.
2. Paisán-Ruíz C, et al. (2004) Cloning of the gene containing mutations that cause PARK8-linked Parkinson's disease. *Neuron* 44:595–600.
3. Zimprich A, et al. (2004) Mutations in LRRK2 cause autosomal-dominant parkinsonism with pleomorphic pathology. *Neuron* 44:601–607.
4. Marín I (2006) The Parkinson disease gene LRRK2: Evolutionary and structural insights. *Mol Biol Evol* 23:2423–2433.
5. Deng J, et al. (2008) Structure of the ROC domain from the Parkinson's disease-associated leucine-rich repeat kinase 2 reveals a dimeric GTPase. *Proc Natl Acad Sci USA* 105:1499–1504.
6. Greggio E, et al. (2008) The Parkinson disease-associated leucine-rich repeat kinase 2 (LRRK2) is a dimer that undergoes intramolecular autophosphorylation. *J Biol Chem* 283:16906–16914.
7. Sen S, Webber PJ, West AB (2009) Dependence of leucine-rich repeat kinase 2 (LRRK2) kinase activity on dimerization. *J Biol Chem* 284:36346–36356.
8. Dachsel JC, et al. (2010) Heterodimerization of Lrrk1-Lrrk2: Implications for LRRK2-associated Parkinson disease. *Mech Ageing Dev* 131:210–214.
9. Smith WW, et al. (2006) Kinase activity of mutant LRRK2 mediates neuronal toxicity. *Nat Neurosci* 9:1231–1233.
10. West AB, et al. (2005) Parkinson's disease-associated mutations in leucine-rich repeat kinase 2 augment kinase activity. *Proc Natl Acad Sci USA* 102:16842–16847.
11. Rubinsztein DC (2006) The roles of intracellular protein-degradation pathways in neurodegeneration. *Nature* 443:780–786.
12. Singleton AB (2005) Altered alpha-synuclein homeostasis causing Parkinson's disease: The potential roles of dardarin. *Trends Neurosci* 28:416–421.
13. Giasson BI, et al. (2002) Neuronal alpha-synucleinopathy with severe movement disorder in mice expressing A53T human alpha-synuclein. *Neuron* 34:521–533.
14. Lee MK, et al. (2002) Human alpha-synuclein-harboring familial Parkinson's disease-linked Ala-53→Thr mutation causes neurodegenerative disease with alpha-synuclein aggregation in transgenic mice. *Proc Natl Acad Sci USA* 99:8968–8973.
15. Chandra S, Gallardo G, Fernández-Chacón R, Schlüter OM, Südhof TC (2005) Alpha-synuclein cooperates with CSPalpha in preventing neurodegeneration. *Cell* 123: 383–396.
16. Hardy J, Lewis P, Revesz T, Lees A, Paisan-Ruiz C (2009) The genetics of Parkinson's syndromes: A critical review. *Curr Opin Genet Dev* 19:254–265.
17. Biskup S, et al. (2007) Dynamic and redundant regulation of LRRK2 and LRRK1 expression. *BMC Neurosci*, 8:102. Available at: http://www.biomedcentral.com/1471-2202/8/102.
18. Fujiwara H, et al. (2002) Alpha-synuclein is phosphorylated in synucleinopathy lesions. *Nat Cell Biol* 4:160–164.
19. Keller JN, et al. (2004) Autophagy, proteasomes, lipofuscin, and oxidative stress in the aging brain. *Int J Biochem Cell Biol* 36:2376–2391.
20. Kabeya Y, et al. (2000) LC3, a mammalian homologue of yeast Apg8p, is localized in autophagosome membranes after processing. *EMBO J* 19:5720–5728.
21. Kirisako T, et al. (1999) Formation process of autophagosome is traced with Apg8/Aut7p in yeast. *J Cell Biol* 147:435–446.
22. Mizushima N, Yoshimori T, Levine B (2010) Methods in mammalian autophagy research. *Cell* 140:313–326.
23. Komatsu M, et al. (2005) Impairment of starvation-induced and constitutive autophagy in Atg7-deficient mice. *J Cell Biol* 169:425–434.
24. Komatsu M, et al. (2007) Homeostatic levels of p62 control cytoplasmic inclusion body formation in autophagy-deficient mice. *Cell* 131:1149–1163.
25. Westerlund M, et al. (2008) Developmental regulation of leucine-rich repeat kinase 1 and 2 expression in the brain and other rodent and human organs: Implications for Parkinson's disease. *Neuroscience* 152:429–436.
26. Beglopoulos V, et al. (2004) Reduced beta-amyloid production and increased inflammatory responses in presenilin conditional knock-out mice. *J Biol Chem* 279: 46907–46914.
27. Bonifati DM, Kishore U (2007) Role of complement in neurodegeneration and neuroinflammation. *Mol Immunol* 44:999–1010.
28. Anglade P, et al. (1997) Apoptosis and autophagy in nigral neurons of patients with Parkinson's disease. *Histol Histopathol* 12:25–31.
29. McNaught KS, Olanow CW, Halliwell B, Isacson O, Jenner P (2001) Failure of the ubiquitin-proteasome system in Parkinson's disease. *Nat Rev Neurosci* 2:589–594.
30. Hara T, et al. (2006) Suppression of basal autophagy in neural cells causes neurodegenerative disease in mice. *Nature* 441:885–889.
31. Komatsu M, et al. (2006) Loss of autophagy in the central nervous system causes neurodegeneration in mice. *Nature* 441:880–884.
32. Pua HH, Dzhagalov I, Chuck M, Mizushima N, He YW (2007) A critical role for the autophagy gene Atg5 in T cell survival and proliferation. *J Exp Med* 204:25–31.
33. Korolchuk VI, Mansilla A, Menzies FM, Rubinsztein DC (2009) Autophagy inhibition compromises degradation of ubiquitin-proteasome pathway substrates. *Mol Cell* 33: 517–527.
34. West AB, et al. (2007) Parkinson's disease-associated mutations in LRRK2 link enhanced GTP-binding and kinase activities to neuronal toxicity. *Hum Mol Genet* 16: 223–232.
35. Li X, et al. (2010) Enhanced striatal dopamine transmission and motor performance with LRRK2 overexpression in mice is eliminated by familial Parkinson's disease mutation G2019S. *J Neurosci* 30:1788–1797.
36. Li Y, et al. (2009) Mutant LRRK2(R1441G) BAC transgenic mice recapitulate cardinal features of Parkinson's disease. *Nat Neurosci* 12:826–828.
37. Lin X, et al. (2009) Leucine-rich repeat kinase 2 regulates the progression of neuropathology induced by Parkinson's-disease-related mutant alpha-synuclein. *Neuron* 64:807–827.
38. Tong Y, et al. (2009) R1441C mutation in LRRK2 impairs dopaminergic neurotransmission in mice. *Proc Natl Acad Sci USA* 106:14622–14627.